JOURNAL OF GEOPHYSICAL RESEARCH, VOL. 100, NO. A4, PAGES 5691–5703, APRIL 1, 1995

Intensities and polarization rates of whistler mode VLF signals observed from a ground network near $L = 4$

M. Ikeda
Section of General Education, Musashi University, Nerima-ku, Tokyo, Japan

I. Nagano and T. Shimbo
Department of Electrical and Computer Engineering, Kanazawa University, Kanazawa, Japan

D. L. Carpenter
STAR Laboratory, Stanford University, Stanford, California

Abstract. VLF signals transmitted from Siple station in Antarctica that propagated through the ionosphere and magnetosphere to the northern hemisphere and triggered emissions generated by the Siple signals in the magnetosphere are radiated from wave exit areas on the ionospheric lower boundary. The locations and extent of the wave exit areas are deduced from the wave intensity distributions measured on the ground. In this method we use measurements of wave magnetic intensity made simultaneously at six stations. The validity of this method is assessed by comparing the results with values simply estimated from a mathematical evaluation and with results of full wave calculations carried out by Nagano et al. (1986, 1987). We find close agreement among results obtained from the three methods and conclude that the wave intensity distribution analysis is valid. The observed distribution of polarization rate also agrees well with the results of the full wave calculations carried out by Nagano et al. (1986, 1987) and with those obtained by the mathematical evaluation. As a result of analyzing a triggered emission in detail, the extent of the wave exit area of the downgoing triggered emission is estimated to be 25–50 km or so at an altitude of 80 km. We believe that this value relates to the horizontal extent of the duct through which the triggered emission propagated in the magnetosphere and ionosphere and that essentially only direct waves transmitted from the wave source arrive within a range of 200 km from the wave intensity peak on the ground.

1. Introduction

In the past the locations in space of wave sources and the properties of wave propagation paths have frequently been studied through determination of wave vectors, Poynting vectors, or wave distribution functions from in situ measurements of magnetospheric and ionospheric VLF emissions. Furthermore, the locations on the ionospheric lower boundary of the exit areas of VLF waves that have propagated through the magnetosphere and ionosphere and the arrival directions of the waves as received on the ground have also been investigated through wave data acquired at ground stations during the past 20 years or more. These studies have sought to make clear the propagation and generation mechanism of VLF waves and also to clarify dynamics and structure of the magnetosphere and ionosphere.

There are several types of techniques to determine arrival directions of VLF waves received on the ground. The first technique is the goniometer method in which arrival directions are assumed to be the directions of the minor axes of polarization ellipses formed from two horizontal components of magnetic fields of VLF waves at the ground [*Bullough and Sagredo*, 1973; *Sagredo and Bullough*, 1973; *Ladwig and Hughes*, 1989]. Since the goniometer method shows only the azimuthal angles of the arrival directions, triangulation by using two observation stations or more is necessary to determine the locations of the wave exit points on the ionospheric lower boundary. Results obtained from triangulation were shown by *Madden et al.* [1978], *Matthews et al.* [1979], *Hayakawa et al.* [1981b, c], *Strangeways et al.* [1982], *Smith and Carpenter* [1982], and *Hayakawa et al.* [1990]. The second method is the technique by which azimuthal angles of arrival directions are determined from horizontal components of Poynting vectors of VLF waves observed on the ground. *Leavitt et al.* [1978] and *Carpenter* [1980] used this method to analyze Siple, Antarctica, VLF transmitter signals propagating through the magnetosphere and ionosphere. The third method can determine both azimuthal and zenith angles of wave vectors of VLF waves emitted into the atmosphere [*Tsuruda and Hayashi*, 1975; *Okada et al.*, 1977, 1981]. By this method, locations of VLF wave exit points on the ionospheric lower boundary were determined [*Ondoh et al.*, 1979; *Tsuruda and Ikeda*, 1979; *Hayakawa et al.*, 1981a, c; *Ohta et al.*, 1984; *Hayakawa et al.*, 1986; *Ohta et al.*, 1989; *Xu et al.*, 1989; *Hayakawa et al.*, 1990].

There are methods in which not only arrival directions but also locations and extent of exit areas on the ionospheric lower boundary of VLF waves observed on the ground are

Paper number 94JA02933.
0148-0227/95/94JA-02933$05.00

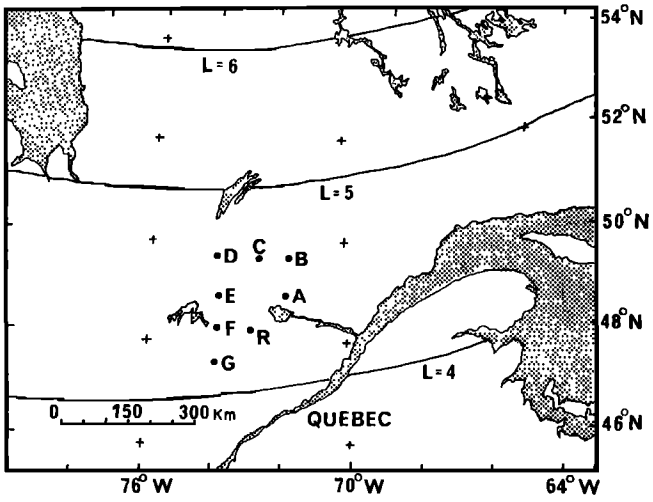

Figure 1. Map showing the locations of the seven stations (A–G) near Roberval, Quebec. The mark R gives the location of Roberval. The longitude of the Siple station geographic conjugate location is about 74°W, and the geographic latitude is about 49°N.

directly determined. One method involves determining exit points from the time difference of wave arrival at two or more stations [e.g., *Nishino et al.*, 1981; *Tanaka and Nishino*, 1988]. Another method involves determining the locations and extent of wave exit areas on the ionospheric lower boundary from the magnetic intensity distributions of VLF waves observed on the ground. This method was used by *Tsuruda et al.* [1982], *Machida and Tsuruda* [1984], and *Ikeda et al.* [1988].

In this paper we briefly present a method of determining the locations and extent of wave exit areas from measurements of the magnetic intensity distribution of VLF waves. We also present two-dimensional distributions of wave intensity and wave polarization rate measured on the ground and compare them with results of model calculations carried out by the full wave technique of *Nagano et al.* [1986, 1987] and with values estimated from the equations of a localized wave source model. By these comparisons the validity of the method of determining the locations and extent of wave exit areas on the ionospheric lower boundary from wave intensity distribution on the ground is assessed, and the errors introduced by this method are also presented. Furthermore, we show that the extent of the exit area of a downgoing triggered emission was 25–50 km or so at an altitude of 80 km and that the distributions of intensity and polarization rate measured on the ground are essentially produced only by the direct waves radiated from a localized wave source.

2. Wave Intensity Distribution Analysis

The method of analysis used in this paper is the same as the one applied by *Ikeda et al.* [1988] to VLF wave data received at Roberval in Canada. We will explain the method for the purpose of clarification.

2.1. Presentation of Analysis Method

The stations were at the seven points (A, B, C, D, E, F, and G) near Roberval in Quebec, Canada, as shown in Figure 1. The data obtained at station C were not accurate and were not used in the analysis. Distances between adjacent stations were about 75 km as indicated by the distance scale. Roberval is located near the geomagnetic conjugate of the Siple station. The L value of Roberval is about 4.

VLF wave data used in this analysis were received on July 23, 1979. Two horizontal components of the magnetic fields of the VLF waves were measured at the six stations by two crossed loop antennae. Using a 25-kHz sampling clock, the two field components were digitized and converted into quantities in frequency space by a 1024-point complex fast Fourier transform. We took the northward complex Fourier component of the wave magnetic field as H_x and the eastward complex Fourier component as H_y and computed $|H_x|^2 + |H_y|^2$ for a 24-Hz frequency interval each 20 ms. All values of $|H_x|^2 + |H_y|^2$ in a rectangle surrounding a signal of interest on a spectrogram were summed for each station, and this quantity was taken as the magnetic intensity $I_{a,\mathrm{obs}}$ of the signal received at station a.

In this wave intensity distribution analysis we determined the location and extent of the wave exit area on the ionospheric lower boundary from the wave magnetic intensity $I_{a,\mathrm{obs}}$ measured at each station. The parameter h is the altitude of the ionospheric lower boundary assumed to be 80 km. This altitude was chosen as a lower limit of the dynamo region because VLF waves below this altitude are approximately characteristic of propagation in free space. First, we assume that a wave source is located somewhere on the ionospheric lower boundary as shown in Figure 2. The X direction is northward, and the Y direction eastward. The distribution of the wave magnetic intensity in the wave source assumed is a Gaussian distribution with attenuation rates different for the north-south and east-west directions. The parameters specifying the wave source are the location of the wave source center (x_0, y_0), the characteristic length to express the size of the wave source (D_x, D_y), and the wave magnetic field intensity at the center of the wave source I. We varied the values of these parameters to search out a parameter set which gives a wave intensity distribution best fitting the distribution observed on the ground and

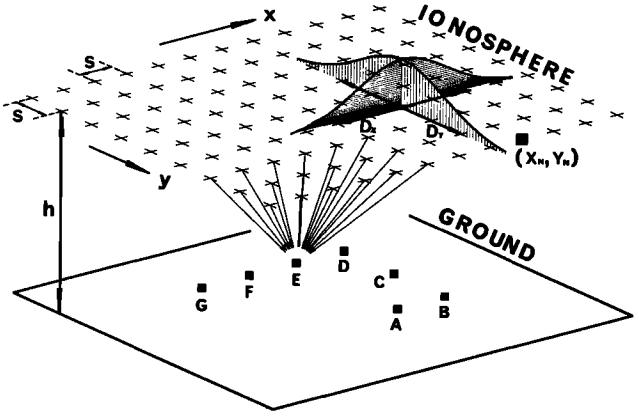

Figure 2. Model of the wave source or wave exit area used in the analysis. The source is located on the ionospheric lower boundary, assumed to be at an altitude of 80 km. The location and extent of the wave source are calculated from the wave magnetic fields measured at six stations.

hence an estimate of a real exit area on the ionospheric lower boundary of a downgoing wave mode.

It is necessary to assume some characteristics for the VLF wave sources. We assume that the radiation obeys Huygens' principle for an electromagnetic wave in free space, and integral equations give a distribution of wave magnetic intensity on the ground through application of the boundary element method. To be more precise, a wave source is separated into many discrete elements, and the magnetic fields of the VLF waves radiated from the element sources are summed up at each observation station as a sum of complex vectors.

The vector potentials $\mathbf{A}_m(\mathbf{r}_{an})$ and $\mathbf{A}_e(\mathbf{r}_{an})$ made at the station a by the element n are expressed as follows:

$$\mathbf{A}_m(\mathbf{r}_{an}) = \frac{\varepsilon_0}{4\pi}(-\mathbf{e}_z) \times \mathbf{E}_n \int d\mathbf{r}' \frac{\exp(-ik_0|\mathbf{r}_{an}-\mathbf{r}'|)}{|\mathbf{r}_{an}-\mathbf{r}'|} \quad (1)$$

$$\mathbf{A}_e(\mathbf{r}_{an}) = -\frac{\mu_0}{4\pi}(-\mathbf{e}_z) \times \mathbf{H}_n \int d\mathbf{r}' \frac{\exp(-ik_0|\mathbf{r}_{an}-\mathbf{r}'|)}{|\mathbf{r}_{an}-\mathbf{r}'|} \quad (2)$$

The parameters ε_0, μ_0, and k_0 are the dielectric constant, the magnetic permeability, and the wave number in free space, respectively. The subscript a identifies the observation station, A, B, D, E, F, or G. The parameter $\mathbf{e}_z$ is a unit vector directed to positive z. The parameter $\mathbf{r}_{an}$ is the vector directed from the center of the element n to the station a and is expressed as follows:

$$\mathbf{r}_{an} = (x_{an}, y_{an}, h) \quad (3)$$

The parameters $\mathbf{E}_n$ and $\mathbf{H}_n$ are the electric and magnetic fields on the element n, respectively. The parameter $\mathbf{r}'$ is the vector directed from the center of the element n to a point on the element n. The plane integrals are done by $\mathbf{r}'$ over the whole element n. The magnetic field of the wave received at the observation station a can be calculated from the vector potentials $\mathbf{A}_m$ and $\mathbf{A}_e$ as follows:

$$\mathbf{H}_{an} = -i\omega\{\mathbf{A}_m + \text{grad}(\text{div}\,\mathbf{A}_m)/k_0^2\} + \text{rot}\,\mathbf{A}_e/\mu_0 \quad (4)$$

where the parameter ω is the angular frequency. The parameters $\mathbf{E}_n$ and $\mathbf{H}_n$ on the element n are assumed to be approximately characteristic of the right-hand circular polarized mode.

$$\mathbf{E}_n \cong (\mu_0/\varepsilon_0)^{1/2} H_n(1, -i, c) \quad (5)$$

$$\mathbf{H}_n \cong iH_n(1, -i, d) \quad (6)$$

We suppose that only radiation terms of (4) contribute substantially to the magnetic fields of the waves received at the stations. Calculating (4) by this assumption,

$$\mathbf{H}_{an} = (\varepsilon_0/\mu_0)^{1/2} \frac{\exp(-ik_0 r_{an})}{r_{an}} \frac{\mathbf{r}_{an}}{r_{an}} \times \mathbf{D} \quad (7)$$

$$\mathbf{D} = \left(\frac{\mathbf{r}_{an}}{r_{an}} \times \mathbf{D}_1 + (\mu_0/\varepsilon_0)^{1/2}\mathbf{D}_2\right) \times \frac{\mathbf{r}_{an}}{r_{an}} \quad (8)$$

$$\mathbf{D}_1 = -\frac{\omega\mu_0}{4\pi i}(-\mathbf{e}_z) \times \mathbf{H}_n \int d\mathbf{r}' \exp\left(ik_0 \frac{\mathbf{r}_{an}}{r_{an}} \cdot \mathbf{r}'\right) \quad (9)$$

$$\mathbf{D}_2 = \frac{\omega\mu_0}{4\pi i}(-\mathbf{e}_z) \times \mathbf{E}_n \int d\mathbf{r}' \exp\left(ik_0 \frac{\mathbf{r}_{an}}{r_{an}} \cdot \mathbf{r}'\right) \quad (10)$$

where the parameter r_{an} is the length of the vector $\mathbf{r}_{an}$.

The horizontal components of the received signal, $(\mathbf{H}_{an})_x$ and $(\mathbf{H}_{an})_y$, are made by summing each term of (7) over n, respectively.

$$(\mathbf{H}_{an})_x = \sum_n \frac{\exp(-ik_0 r_{an})}{r_{an}} Q_{an} H_n \quad (11)$$

$$(\mathbf{H}_{an})_y = \sum_n \frac{\exp(-ik_0 r_{an})}{r_{an}} R_{an} H_n \quad (12)$$

$$Q_{an} = \frac{k_0}{4\pi} I_{an}\left\{-\frac{h}{r_{an}}\left(1 + \frac{h}{r_{an}}\right) - i\frac{y_{an}}{r_{an}}\left(\frac{x_{an}}{r_{an}} - i\frac{y_{an}}{r_{an}}\right)\right\} \quad (13)$$

$$R_{an} = \frac{k_0}{4\pi} I_{an}\left\{i\frac{h}{r_{an}}\left(1 + \frac{h}{r_{an}}\right) + i\frac{x_{an}}{r_{an}}\left(\frac{x_{an}}{r_{an}} - i\frac{y_{an}}{r_{an}}\right)\right\} \quad (14)$$

$$I_{an} = \frac{4r_{an}^2}{k_0^2 x_{an} y_{an}} \sin\left(\frac{k_0 x_{an} s}{2r_{an}}\right) \sin\left(\frac{k_0 y_{an} s}{2r_{an}}\right) \quad (15)$$

Accordingly, with the ground assumed to be a perfect reflector, the magnetic intensity obtained at station a, $I_{a,\text{cal}}$, is formed by the signal radiated from a wave source located on the ionospheric lower boundary as follows:

$$I_{a,\text{cal}} = \sum_n (1/r_{an}^2)(|Q_{an}|^2 + |R_{an}|^2)|H_n|^2 \quad (16)$$

where we assumed that the effect of interference among waves emitted from all elements was negligible because of phase mixing. Substituting (13) and (14) for (16),

$$I_{a,\text{cal}} = \sum_n \frac{k_0^2}{16\pi^2} \frac{I_{an}^2}{r_{an}^2}\left(1 + \frac{h^2}{r_{an}^2}\right)\left(1 + \frac{h}{r_{an}}\right)^2 |H_n|^2 \quad (17)$$

Equation (17) is applied to the analysis of the wave intensity distribution on the ground. The parameter I_{an} is approximately given by

$$I_{an} \cong s^2 \quad (18)$$

where the parameter s is a coherent length equivalent to the side length of a source element and set to 50 km. Furthermore, the relation for $|H_n|^2$ is assumed to be as follows:

$$|H_n|^2 = I \exp\left\{-\frac{(x_n - x_0)^2}{D_x^2} - \frac{(y_n - y_0)^2}{D_y^2}\right\} \quad (19)$$

2.2. Analyses of a Triggered Emission

In this subsection we show an example of results obtained by analyses of wave magnetic intensity distributions on the ground. The emission which was triggered by a Siple signal and then received at station F is shown in the spectrogram of Figure 3a. The analyzed portion is the region inside the rectangle. The exit area on the ionospheric lower boundary from which the triggered emission was found to be emitted is shown in Figure 3b. The exit area of this triggered emission was located just southeast of station G, and its extent was 25

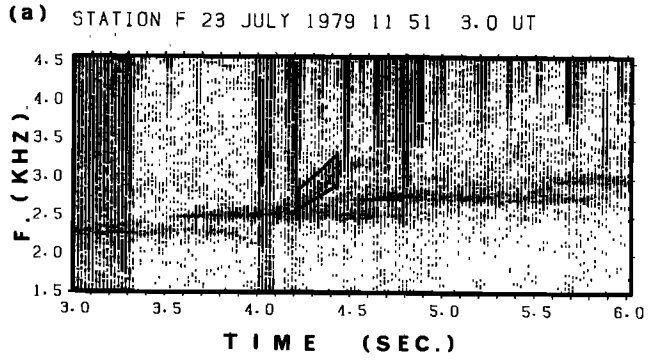

Figure 3a. Dynamic spectrum of VLF signals observed at station F. The frequency of the triggered emission analyzed within the time interval of 0.2 s is about 3.0 kHz. The dark portion between 3.0 and 3.3 s is due to automatic gain control.

km in the north-south direction (D_x) and 50 km in the east-west direction (D_y). The exit area was a localized source of VLF wave radiation, since the wave length is about 100 km, which is greater than the horizontal scale of this exit area.

The distributions of intensity and polarization rate of the wave magnetic fields observed on the ground are shown in Figures 4 and 5, respectively. In Figure 4a the circles correspond to the magnetic field intensities measured at stations E and A, while the crosses correspond to the wave magnetic field intensities measured at stations D and B. Figure 4b shows wave magnetic field intensities measured at stations G, F, E, and D. The dashed and solid lines in Figures 4a and 4b express wave intensity distributions of magnetic fields computed from the wave source shown in Figure 3b. Their lines agree with the observed values very well. The horizontal axes in Figures 4a and 4b correspond to a distance of 300 km.

The polarization rate P is defined as follows:

$$P = (R - L)/(R + L) \tag{20}$$

The parameter R is the amplitude of the right-handed circular component of a wave horizontal magnetic field measured at an observation station, while L represents the left-handed circular component. However, the polarization rates shown in Figure 5 represent an intensity-weighted average $\bar{P}$ over the rectangle in Figure 3a, as given by the following equation:

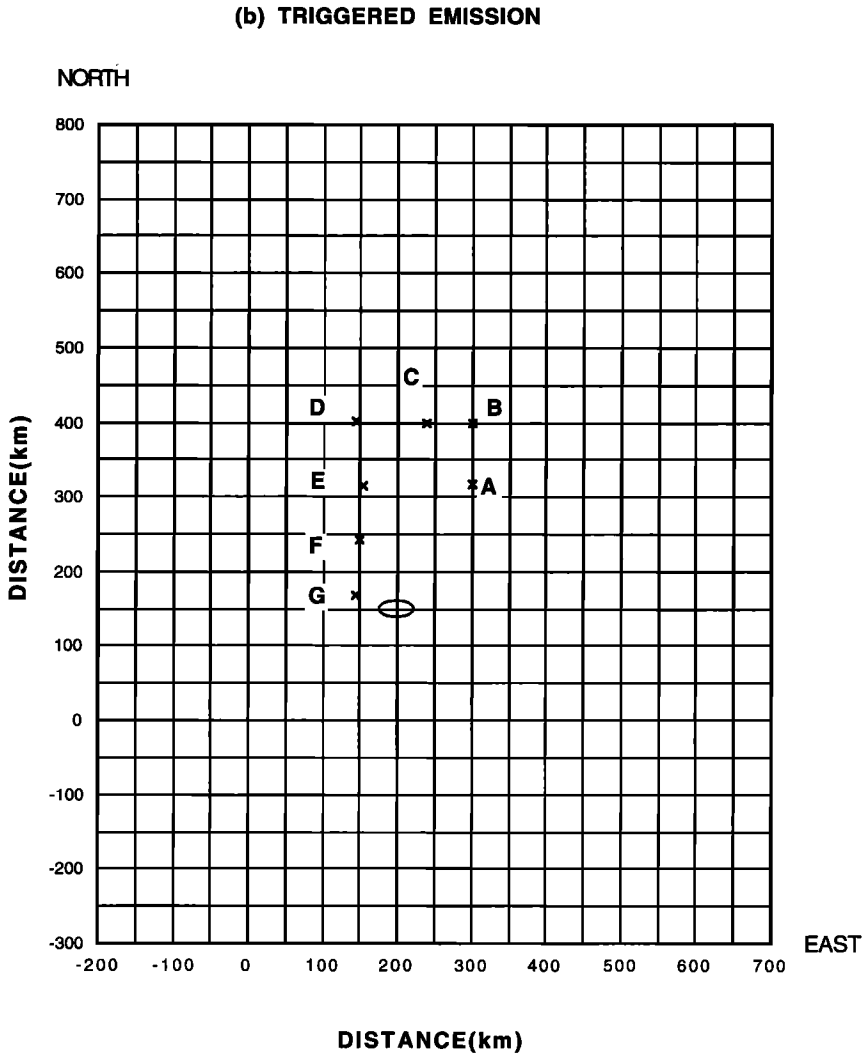

Figure 3b. Wave exit area determined from the wave intensity distribution analysis of the triggered emission. The upward direction corresponds closely to geomagnetic north, the right side closely to geomagnetic east. The side length of one regular square is 50 km.

$$\bar{P} = \left(\sum_c P_c I_c\right) \Big/ \sum_c I_c \tag{21}$$

The parameter P_c is a polarization rate computed in each frequency-time cell 24 Hz × 20 ms in extent on the spectrogram shown in Figure 3a, while the parameter I_c is the magnetic field intensity computed in the corresponding cell. The vertical bars shown in Figure 5 express the deviation of polarization rate $\overline{\Delta P}$ from the averaged value at each station, defined as follows:

$$\overline{\Delta P} = \left(\left[\sum_c (P_c - \bar{P})^2 I_c\right] \Big/ \sum_c I_c\right)^{1/2} \tag{22}$$

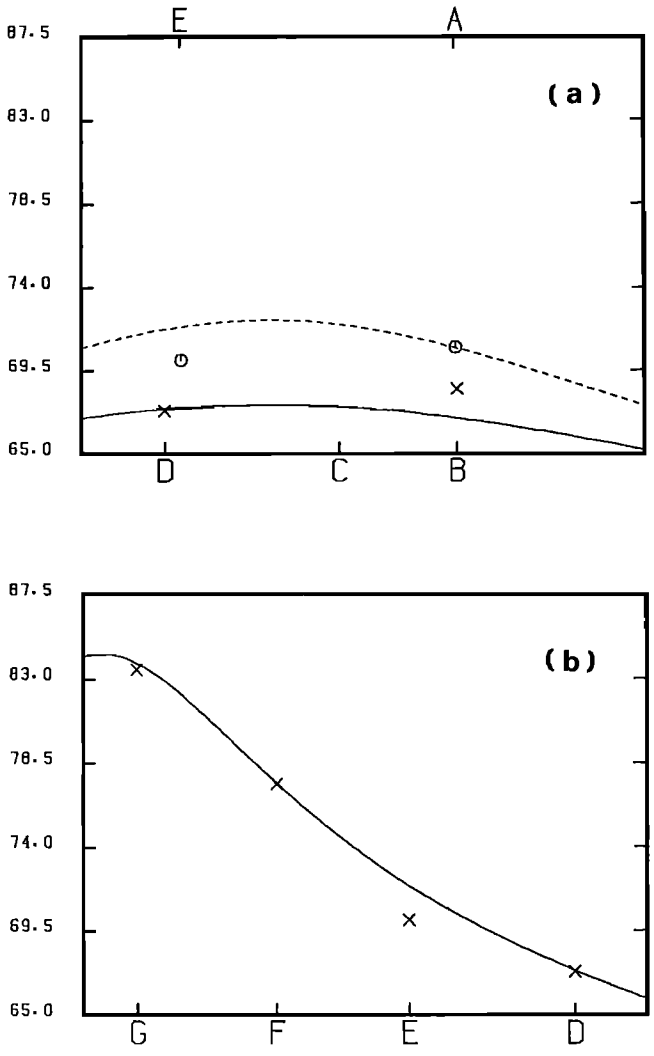

Figure 4. (a) Spatial distribution in the east-west direction of the magnetic intensity of the triggered emission shown in Figure 3. The vertical axis represents wave magnetic intensity in decibels, but the value corresponding to 0 dB is arbitrary. The lower horizontal axis represents distance along a longitudinal line passing near stations D, C, and B, and the upper horizontal axis represents distance along a longitudinal line passing near stations E and A. (b) Spatial distribution in the north-south direction of magnetic intensity of the triggered emission shown in Figure 3. The vertical axis is the same as that of the Figure 4a, but the horizontal axis represents distance along a meridian near stations G, F, E, and D.

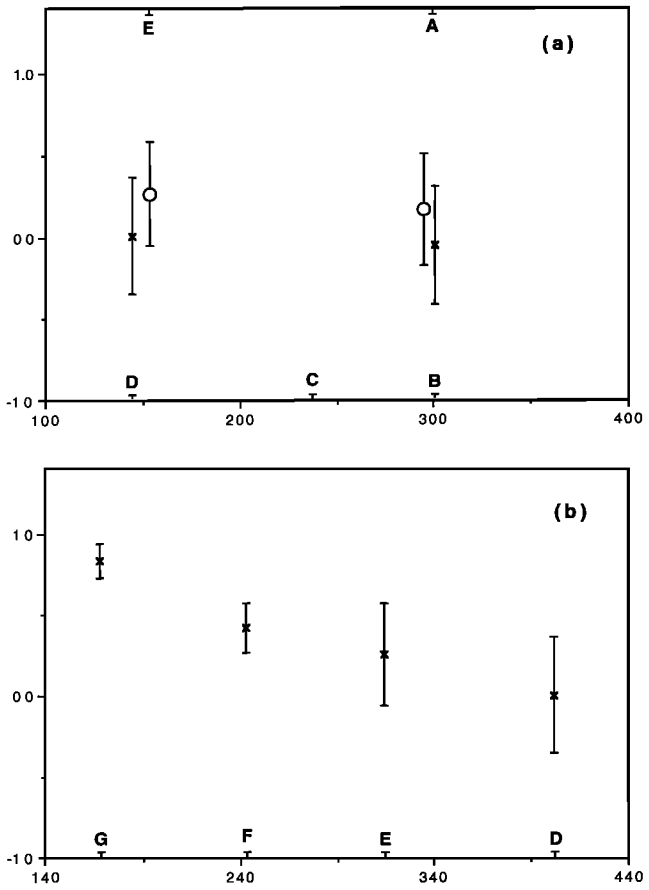

Figure 5. (a) Spatial distribution in the east-west direction of the polarization rate of the triggered emission shown in Figure 3. The polarization rates at stations E and A are denoted by circles and those observed at stations D and B are denoted by crosses. (b) Spatial distribution in the north-south direction of the polarization rate of the triggered emission shown in Figure 3. The format of this figure is the same as in Figure 5a, but the horizontal axis corresponds to distance along a meridian near stations G, F, E, and D.

The vertical axes in Figures 5a and 5b express $\bar{P}$; a right-hand circularly polarized wave corresponds to $\bar{P} = 1.0$, a linear wave to $\bar{P} = 0.0$, and a left-hand circularly polarized wave to $\bar{P} = -1.0$. The dashed and solid bars correspond to the data of stations A and E, and B and D, respectively.

The results obtained through the analysis of this triggered emission are not unusual. To illustrate, we present some results for a whistler mode emission received at the station network. The results are illustrated in Figures 6a and 6b, where the spectrogram and wave exit area of the whistler mode emission are shown, and in Figures 7 and 8, where the intensity distribution and polarization rate distribution of the whistler mode emission are shown. The formats of Figures 7 and 8 are the same as those used in Figures 4 and 5.

The frequency of the whistler mode emission was about 4.5 kHz, which is higher than the ~3.0-kHz frequency of the triggered emission described before. The wave exit area of the whistler mode emission was located about 20 km to the south of station G, or approximately the location of the wave exit area of the triggered emission. The extent of the wave exit area of the whistler mode emission was 50 km in the north-south direction (D_x). The whistler mode emissions received at stations A, B, D, and E appear to have been

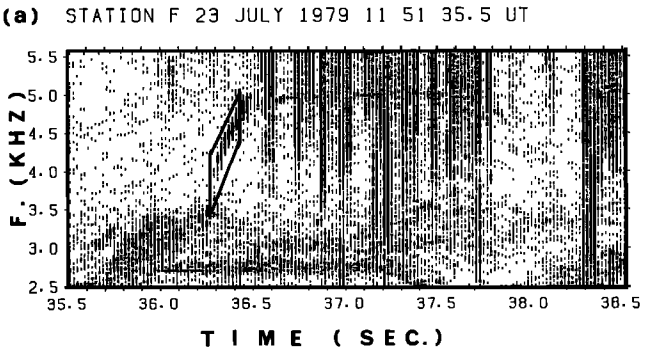

Figure 6a. Dynamic spectrum of a whistler mode emission observed at station F. The format is the same as in Figure 3.

hidden in various noise activity at these stations because the intensities were almost same.

On the whole the results obtained from these analyses show that the characteristics found in the triggered emission were repeated in Figures 6, 7, and 8. We thus believe that both the triggered emission and the whistler mode emission propagated along the same single duct and hence that these signals were not affected by the interference of waves transmitted from two or more wave exit areas.

3. Full Wave Calculation

In this section we will compare the distributions of intensity and polarization rate of the wave magnetic field shown in Figures 4 and 5 with results of full wave calculations using the method developed by *Nagano et al.* [1986, 1987]. One of the results is shown in Figure 9, where the whistler waves with frequency of 3.00 kHz, close to the frequency of the triggered emission of Figure 3a, are incident from an altitude of 110 km as a beam wave and then form an intensity distribution of wave magnetic field on the ground.

The height distribution of electron number density was obtained from the profile shown in Figure 7 of *Mechtly* [1974]. The profile is the height distribution of electron number density selected in relation to the zenith angle of the sun during this observation. The cyclotron frequency of electrons was assumed to be 1.2 MHz, and the dip angle of the magnetic field line was assumed to be 75° in the ionosphere. The effective collision frequency was derived from atmospheric pressure of the COSPAR International Refer-

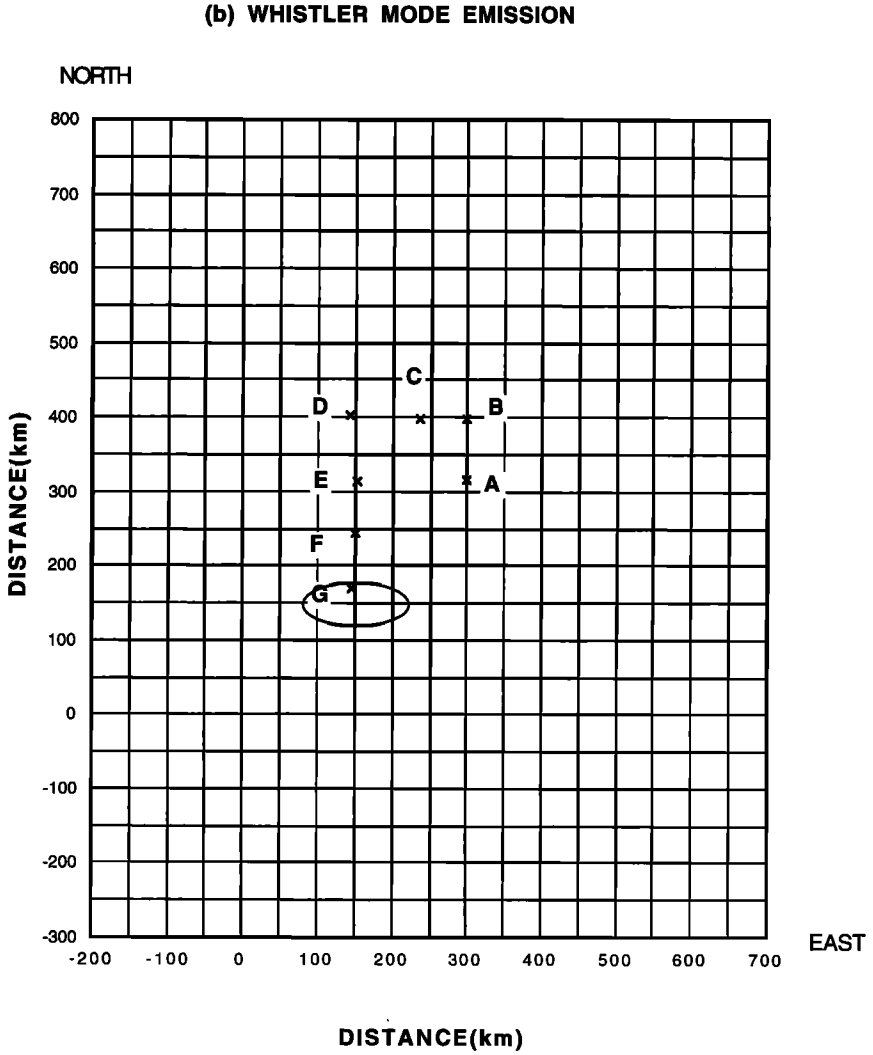

Figure 6b. Wave exit area of the whistler mode emission. The format is the same as in Figure 3.

ence Atmosphere model [*Nagano et al.*, 1982]. The conductivity and relative dielectric constant of the ground were assumed to be $\sigma = 1$ mS/m and $\varepsilon^* = 10$, respectively. A change in the ground conductivity has a negligible effect on the results.

The beam wave used in this mode calculation is the wave that comprises many whistler mode plane waves with different **k** vectors. The propagation of each plane wave is computed by the full wave method of *Nagano et al.* [1986, 1987]. In this calculation it is necessary to use a spectrum distribution of **k** vectors of whistler mode waves propagating from the incident altitude. The incident angles of the input whistler mode waves propagating downward from the lower ionosphere to the ground are inside the cone formed by the angle called the transmission angle (θ), which is given by Snell's law as $\theta = \sin^{-1}(1/\mu)$, where μ is the real part of the whistler mode refractive index at the incident altitude. We assume that of all whistler mode waves transmitted from a duct in this ionosphere, only waves propagating within the transmission cone can reach the ground. Furthermore, it is assumed that the **k** spectrum of these whistler mode waves is uniform within the transmission cone and that the power density affecting the intensity distribution is zero outside this cone.

The plane whistler mode waves with different **k** vectors are Fourier synthesized in wave number space. As a result,

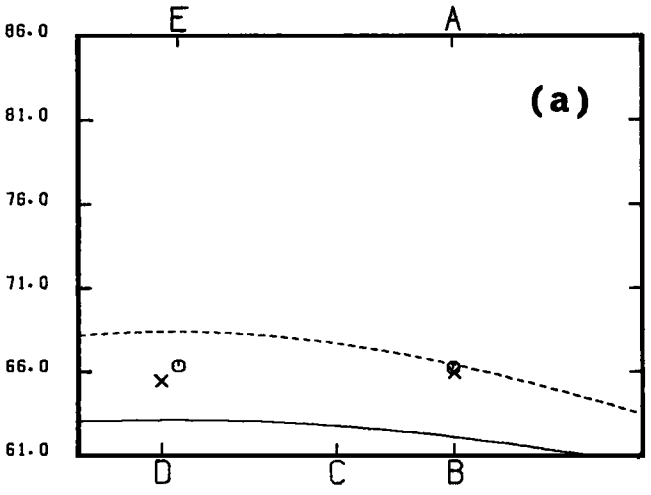

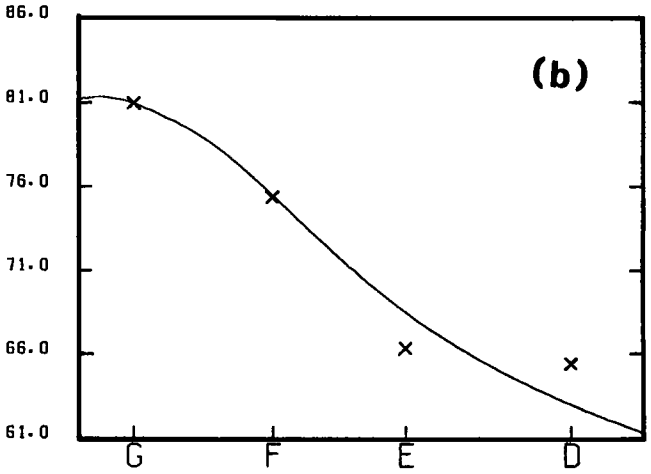

Figure 7. Wave intensity distribution on the ground obtained from the analysis of the whistler mode emission shown in Figure 6. The format of this figure is the same as in Figure 4.

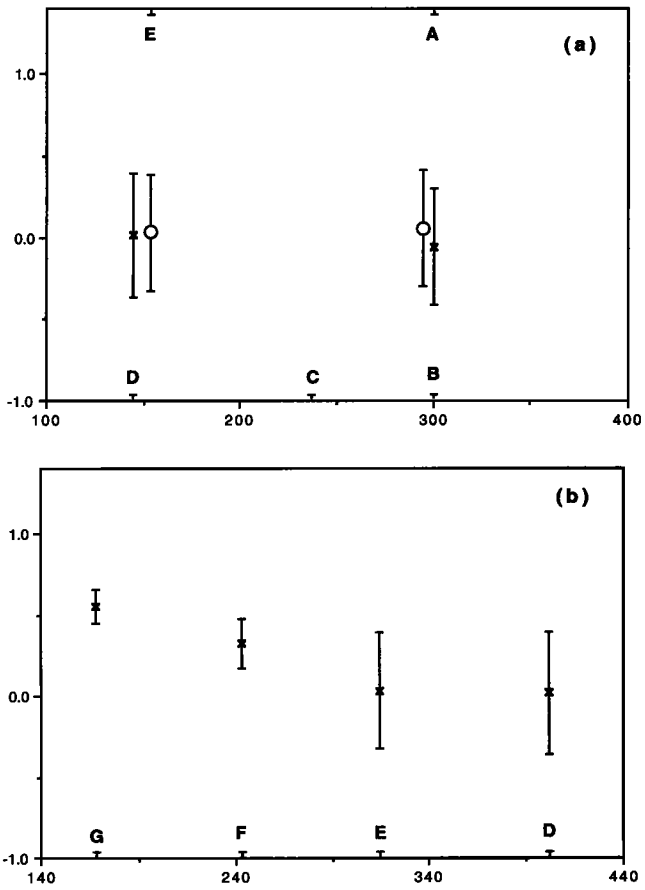

Figure 8. Polarization rates observed on the ground for the whistler mode emission shown in Figure 6. The format of this figure is the same as in Figure 5.

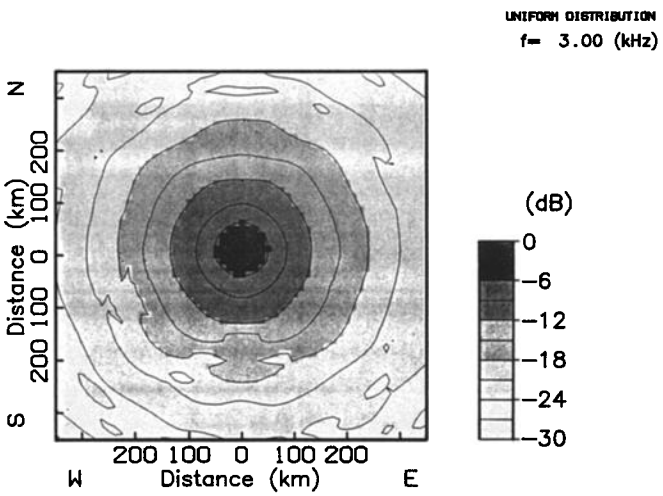

Figure 9. Intensity distribution of the wave magnetic field ($|H|^2$) obtained from the model calculations carried out by the full wave method of *Nagano et al.* [1986, 1987].

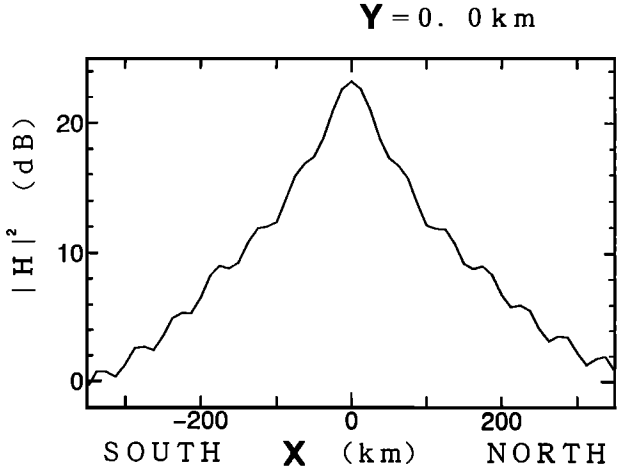

Figure 10. Intensity profile on the line passing through the origin in the north-south direction in reference to the two-dimensional intensity distribution shown in Figure 9. The vertical axis expresses intensity from 0 to 20 dB and the horizontal axis expresses distance in kilometers.

the minimum distance scale digitized on the ground, namely the distance resolution, becomes about 12.5 km in both the east-west and north-south directions. The results are shown in Figure 9, which shows contour lines of the magnetic field intensities in a range within 350 km from the intensity peak on the ground. An interval between two adjacent contour lines is 3 dB, and the attenuation from the intensity peak situated at the center to −30 dB intensity is shown with contour lines on the map.

The profile of wave magnetic field intensity as a function of distance from the peak in the north-south direction is shown in Figure 10, but the levels corresponding to 0 dB in Figures 9 and 10 are different from each other. The position at $(x, y) = (0, 0)$ is situated at the peak of wave magnetic field intensity on the ground. The wave magnetic field intensity distribution shows an attenuation rate of 8.2 dB/100 km within a range of 200 km from the intensity peak on the ground.

Figure 11 shows the profile of polarization rate as a function of distance from the intensity peak in the north-south direction obtained by model calculations of the full wave technique. It shows an attenuation rate of 0.37/100 km within a range of 200 km from the intensity peak on the ground. In the region over 250 km distant from the intensity peak the polarization rate is negative, meaning that the signals received there become waves corresponding to the left-hand polarized mode. We believe that the left-hand polarized mode is produced because direct waves and waves reflected at the ground and by the ionosphere overlap each other. It is necessary to compare these results with the polarization rate distribution measured at the station network.

4. Comparison

4.1. Mathematical Evaluation

Inferring from the observed results shown in Figure 3 and the results calculated by the full wave technique and shown in Figure 10, we suppose that the extent of the wave exit area located on the ionospheric lower boundary near Roberval is about 50 km. In order to examine the physical characteristics of this wave source model, we will give the mathematical equations representing a wave source model in which the wave exit area is localized with an extent of 50 km. By examining these equations we believe that the physical mechanism of propagation between wave exit areas located on the ionospheric lower boundary and stations on the ground can be understood more clearly. As shown in Figure 3b, the wave source of the triggered emission described in Figure 3a was so small that we could almost regard it as a point source. Accordingly, (17) is approximated as follows:

$$I_{a,\mathrm{cal}} \cong \frac{k_0^2}{16\pi^2}\frac{s^4}{r_{a0}^2}\left(1+\frac{h^2}{r_{a0}^2}\right)\left(1+\frac{h}{r_{a0}}\right)^2 |H_0|^2 + A^2 \qquad (23)$$

In this equation, only one important element of the wave source was used, expressed by the subscript "0." The A^2 expresses the intensity of noise such as effects produced by other wave source elements, interference among a direct wave and waves reflected at the ionospheric lower boundary, atmospherics, and influences of the various approximations introduced into the wave source model. We suppose that it is a constant value independent of the observation station and duration.

Absolute amplitudes of waves received with right-handed and left-handed polarization on the ground, R and L, respectively, are expressed as follows:

$$R = (1/\sqrt{2})\left|\sum_n (\mathbf{H}_{an})_x + i\sum_n (\mathbf{H}_{an})_y\right| \qquad (24)$$

$$L = (1/\sqrt{2})\left|\sum_n (\mathbf{H}_{an})_x - i\sum_n (\mathbf{H}_{an})_y\right| \qquad (25)$$

Obtaining the squares of R and L and retaining only the term expressing the wave source element with the subscript 0 in accordance with the assumption of a localized wave source,

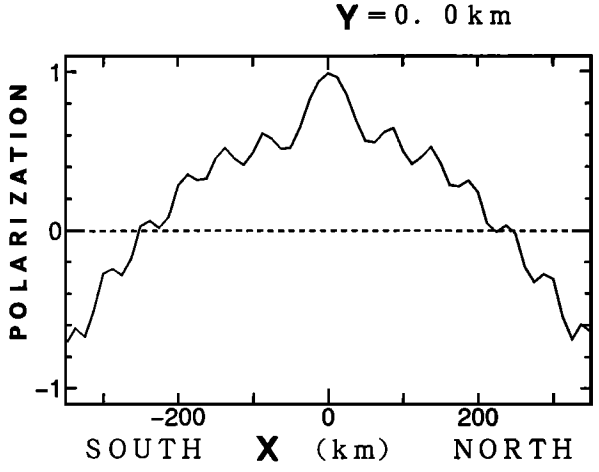

Figure 11. Polarization rate profile on the line passing through the origin in the north-south direction. The vertical axis expresses polarization rate from −1.0 to 1.0, and the horizontal axis distance in kilometers.

$$R^2 \cong \frac{k_0^2}{32\pi^2}\frac{s^4}{r_{a0}^2}\left\{2\frac{h}{r_{a0}}\left(1+\frac{h}{r_{a0}}\right) + \frac{(x-x_0)^2+(y-y_0)^2}{r_{a0}^2}\right\}^2 |H_0|^2 + R_N^2 \quad (26)$$

$$L^2 \cong \frac{k_0^2}{32\pi^2}\frac{s^4}{r_{a0}^2}\left\{\frac{(x-x_0)^2+(y-y_0)^2}{r_{a0}^2}\right\}^2 |H_0|^2 + L_N^2 \quad (27)$$

R_N^2 and L_N^2 are noise intensities of right-hand and left-hand polarized waves, respectively. In the equations described above, the parameters x_0 and y_0 are the northward and eastward components of the position coordinates of the important element with subscript 0, and the parameters x and y are the northward and eastward components, respectively, of the position coordinates on the ground. Ordinarily, one can justify assuming that $A^2 = R_N^2 + L_N^2$, and we suppose that $R_N^2 = L_N^2$ due to a white noise assumption. Then (23), (26), and (27) are reduced as follows:

$$\frac{I_{a,\mathrm{cal}}}{|H_0|^2} \cong \frac{k_0^2}{16\pi^2}\frac{s^4}{r_{a0}^2}\left(1+\frac{h^2}{r_{a0}^2}\right)\left(1+\frac{h}{r_{a0}}\right)^2 + \frac{A^2}{|H_0|^2} \quad (28)$$

$$\frac{R^2}{|H_0|^2} \cong \frac{k_0^2}{32\pi^2}\frac{s^4}{r_{a0}^2}\left\{2\frac{h}{r_{a0}}\left(1+\frac{h}{r_{a0}}\right) + \frac{(x-x_0)^2+(y-y_0)^2}{r_{a0}^2}\right\}^2 + \frac{1}{2}\frac{A^2}{|H_0|^2} \quad (29)$$

$$\frac{L^2}{|H_0|^2} \cong \frac{k_0^2}{32\pi^2}\frac{s^4}{r_{a0}^2}\left\{\frac{(x-x_0)^2+(y-y_0)^2}{r_{a0}^2}\right\}^2 + \frac{1}{2}\frac{A^2}{|H_0|^2} \quad (30)$$

4.2. Observation, Full Wave Calculation, and Mathematical Evaluation

We compared the wave intensities and polarization rates observed at stations A–G with those obtained by the calculations using a full wave technique and by the mathematical model equations for a localized wave source. The results are shown in Figures 12, 13, and 14. We considered both the position coordinates of the magnetic field intensity peak on the ground and the base line level corresponding to 0 dB to be variable and fitted a wave intensity distribution obtained by the full wave calculation model to the one obtained from the observations, varying values of the two parameters. The calculated intensities and polarization rates obtained at the observation stations A–G are given in the three figures.

The position of the intensity peak is shown by a circle in Figure 15. The observed values (crosses) and the computed values (open circles) for intensity and polarization rate at the positions corresponding to stations D, C, and B are shown in Figure 12. The distance between the ends of the abscissa in each panel corresponds to 300 km. The solid lines express the intensity and polarization rate distributions evaluated from (28), (29), and (30) along the longitudinal line passing near stations D, C, and B. The position of the localized wave source used in the mathematical evaluation is assumed to be the same as that of the intensity peak used for the full wave calculations and is shown by a square in Figure 15.

Figure 13 shows that the values are obtained at the positions of stations E and A and along the longitudinal line passing near E and A, while Figure 14 shows the corresponding values for stations G, F, E, and D.

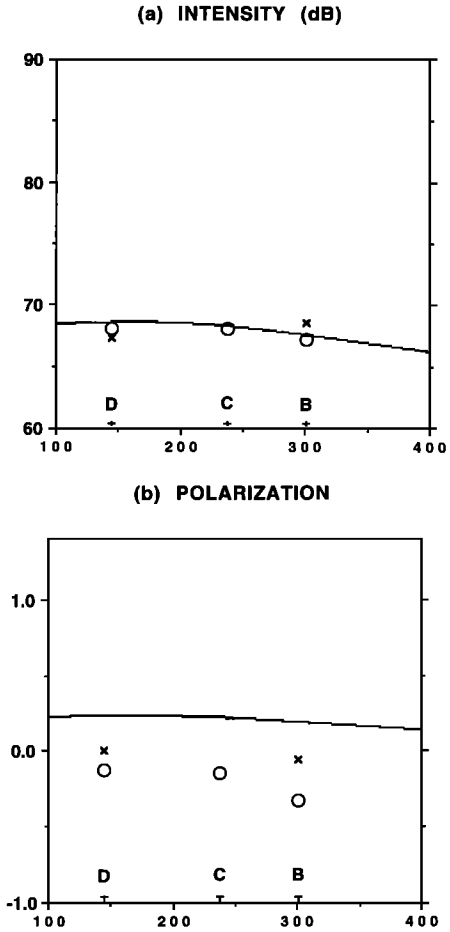

Figure 12. Comparison among results observed at the respective stations (crosses), model calculation results computed so as to best fit the observed results (open circles), and results evaluated mathematically (solid line). The vertical axis expresses (a) intensity in decibel units and (b) polarization rate. Both the horizontal axes express distance along the latitudinal line passing near stations D, C, and B. The level of 0 dB in intensity is arbitrary.

From Figures 12 to 14 we find that the values observed near Roberval, the values computed by the full wave technique, and the values estimated from the mathematical model equations are in good agreement with one another. The attenuation rate of wave intensity between stations G and D was 6.93 dB/100 km in the observations and 6.63 dB/100 km in the full wave calculations.

There was also very good agreement between the position of the wave source obtained by the wave intensity distribution analysis, shown in Figure 3b, and the position of the wave source obtained by the full wave calculations and shown by a circle in Figure 15. However, we found that the position of the wave source obtained by the full wave calculations was shifted westward by 37.5 km from the position of the wave source obtained by the wave intensity distribution analysis. The value of 37.5 km falls within the error tolerance of the wave intensity distribution analysis, since we must take into account an uncertainty of at least ~50 km, the distance interval between two adjacent com-

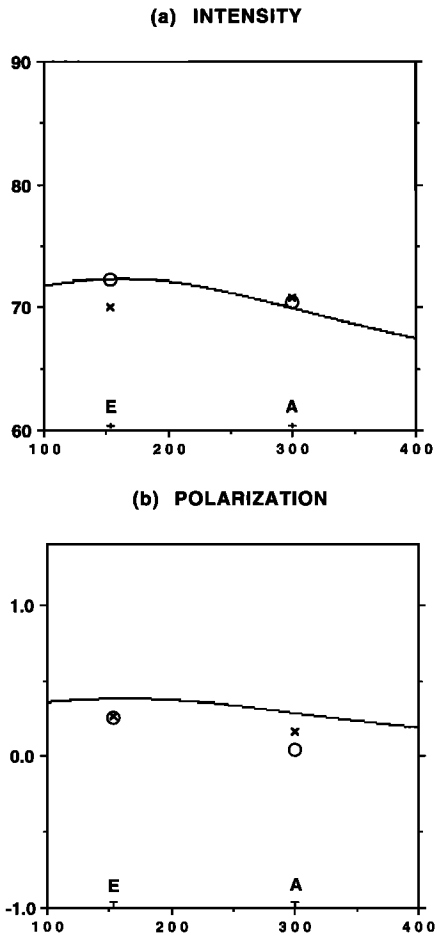

Figure 13. Comparison among observed (crosses), model-calculated (open circles), and mathematically evaluated (solid line) results shown in the format of Figure 12. In both panels the horizontal axes express distance along a latitudinal line passing near stations E and A. (a) Intensity and (b) polarization.

puting points, in applying the wave source model to the wave intensity distribution analysis. This is the case even when the received signals have intensities of sufficient strength and are not influenced by other signals.

Judging from the fact that there is very good agreement between the observed values and the calculated values of polarization rate from G to D, namely 0.35/100 km in the observations and 0.37/100 km in the full wave calculations, it appears likely that the full wave calculation model indicates the actual propagation mechanism of VLF waves transmitted from a duct in the lower ionosphere within a region up to 200 km distant from the wave intensity peak on the ground.

Next we examine the validity of the wave source model applied in the wave intensity distribution analysis. The intensity and polarization rate distributions derived from (28), (29), and (30) are shown by solid lines in Figures 12–14. We assume that the position coordinates of the wave source and the base line level corresponding to 0 dB intensity are both variable and make the evaluated intensity distribution coincide with the observed intensity distribution. The noise level ($A^2/|H_0|^2$) is assumed to be -30 dB. The k_0 in (28)–(30) is calculated from the frequency 3.0 kHz. With the exception of results obtained at stations D and B, these solid lines seem to agree well with the observed values and the full wave calculated values with regard to the distributions of both intensity and polarization rate. The fact that there is a good agreement in polarization rate is worth noting in particular. The difference between the polarization rates obtained at stations B and D and those corresponding to the solid line at these stations indicates that some assumptions of the wave source model are not appropriate to the VLF wave propagation to those stations.

From the results described above we conclude that the wave source model is a reasonable model for a wave source on the ionospheric lower boundary. Since a model wave source with horizontal extent of about 50 km at an altitude of 80 km produces results consistent with observations, we conclude that, with regard to the analyzed triggered emission, the extent of the exit area of a downgoing mode wave at this altitude was actually ~50 km.

5. Discussion and Conclusion

The intensity and polarization rate distributions of a triggered emission and a whistler mode emission observed near Roberval in 1979 have been presented. The inferred

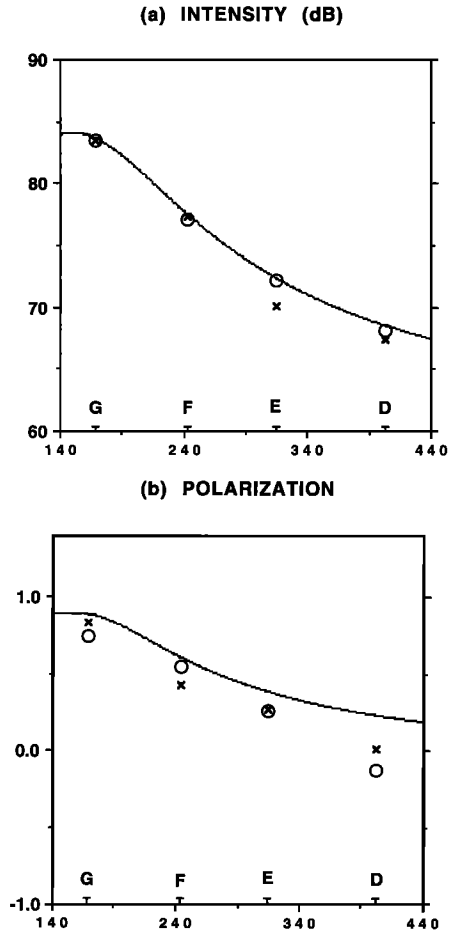

Figure 14. Comparison among observed (crosses) model-calculated (open circles), and mathematically evaluated (solid line) results shown in the format of Figure 12. In both panels the horizontal axes express distance along a meridian line passing near stations G, F, E, and D. (a) Intensity and (b) polarization.

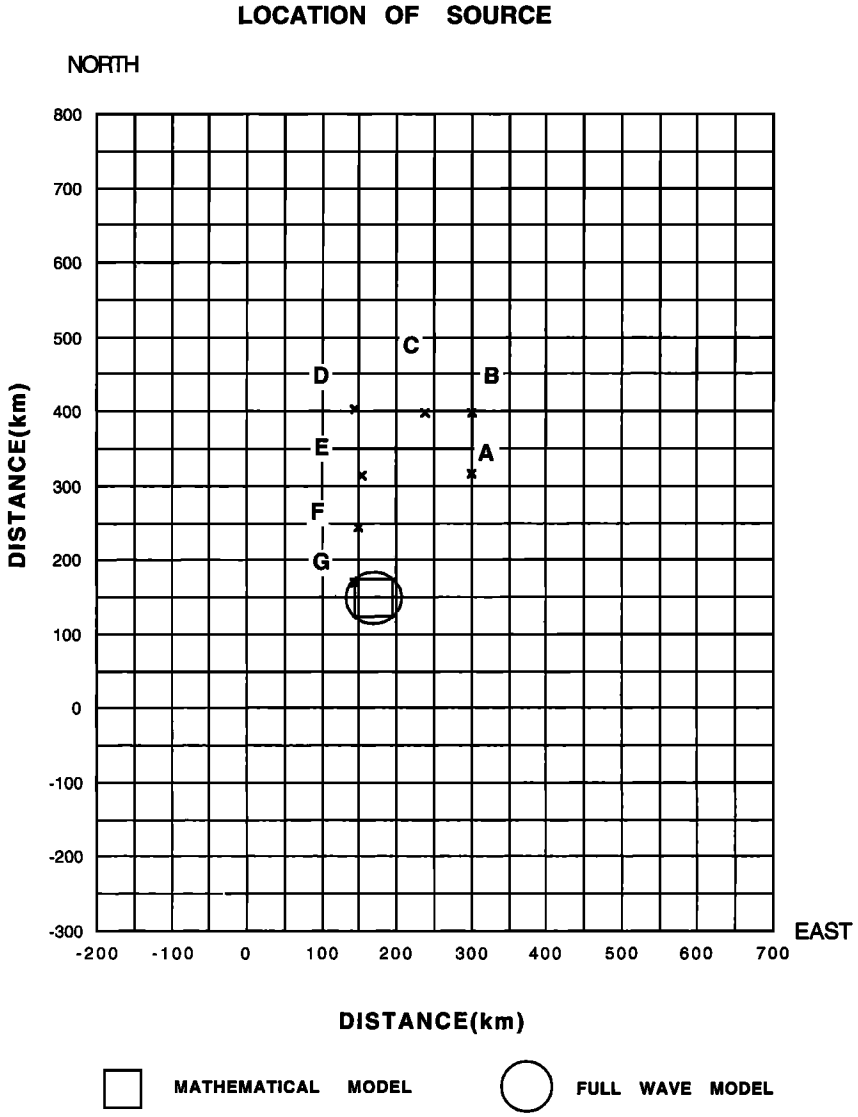

Figure 15. Wave source location determined by the full wave calculations that best fits the observed intensity distribution (circle), and the one assumed in the mathematical evaluation (square). The format of this figure is the same in Figure 3b.

wave exit areas of the triggered emission and the whistler mode emission had horizontal extents of 25–50 km at an altitude of 80 km. However, we cannot conclude that wave exit areas of downgoing whistler mode waves are always 25–50 km in extent at an altitude of 80 km near Roberval. In order to clarify this problem we need to obtain more VLF data at multiple stations and to analyze them exactly.

Model calculations using the full wave technique developed by *Nagano et al.* [1986, 1987] showed that the ground distributions of wave magnetic intensity and polarization rate predicted for whistler beam waves transmitted from a duct end in the lower ionosphere agreed well with the observed distributions. These results show that the attenuation rate of wave magnetic intensity was about 8.2 dB/100 km and that of polarization rate about 0.37/100 km in the region within 200 km distant from the intensity peak on the ground.

To make the computed values coincide with the observed values, we varied the peak position of the wave intensity distribution obtained from model calculations by the full wave technique. We found that the peak was located 37.5 km west of the position of the wave exit area that was obtained from the analysis of the wave intensity distribution on the ground. As a result, we believe that the position of a wave exit area obtained by this wave intensity distribution analysis may be shifted at least ~50 km from the real position of a wave source located on the ionospheric lower boundary 80 km above the ground.

There was clear agreement between the observed values and the values obtained from this full wave calculation. It is likely that this full wave calculation accurately describes the propagation mechanism of whistler mode waves transmitted from a duct in the lower ionosphere into the atmosphere. Hereinafter we would like to examine how the extent of the intensity and polarization rate distributions changes according to the characteristics of the whistler beam wave.

In order to examine the validity of the wave source model used in this wave intensity distribution analysis, we derived

equations expressing VLF waves radiated from a localized wave source 50 km square and compared the results calculated from these equations with observed values. Some results calculated from these equations agreed well with both those obtained from the full wave calculation and those observed near Roberval, and we conclude that the wave source used in this wave intensity distribution analysis was a reasonable model of the actual source. We find that the mathematical equations expressing the model wave source can reproduce the distributions of both observed intensities and polarization rates and from this conclude that essentially only direct waves reach positions on the ground located within 200 km of the intensity peak. The wave fields observed near Roberval were near-source fields.

The extent (50 km) of the wave source at an altitude of 80 km can be considered a very rough measure of the width in the upper ionosphere of the duct along which the analyzed triggered emission was propagating to the vicinity of Roberval. Evidence from whistlers and emissions as well as theory [see *Carpenter*, 1988, and references therein] indicates that whistler mode ducts effectively terminate in the topside ionosphere and that the downcoming wave energy then spreads as it illuminates the lower ionospheric boundary. The wave source (or wave exit) area identified here then becomes that portion of the illuminated boundary region that is effectively penetrated by the waves, the remaining portion being characterized by internal reflection and upward repropagation of the waves.

To determine the location, extent, and wave intensity of a wave exit area on the ionospheric lower boundary, a number of stations on the ground arranged in both the north-south and east-west directions are necessary. By carrying out observations such as those described above and by reducing the distance between the computing points, we should be able to infer with increased accuracy the distributions and shapes of wave exit areas on the ionospheric lower boundary, the distributions and cross-sectional shapes of the ducts through which whistler mode waves propagate in the magnetosphere and ionosphere, and the mechanism of wave propagation in those regions.

Acknowledgments. This research was carried out by using VLF wave data of the Institute of Space and Astronautical Science (ISAS) in Japan and by making use of computer facilities of ISAS, Kanazawa University, Musashi University, and Stanford University. We would like to thank K. Tsuruda for very useful comments, data supply, and convenient computer usage. We also thank S. Machida of Kyoto University very much for cooperation in data processing and in the use of computer facilities and computer program resources. Furthermore, one of us (M.I.) greatly appreciates the kindness and cooperation of many colleagues at Musashi University and the help of many people at Stanford University during a recent visit. The work at Stanford was supported by the Division of Polar Programs of the National Science Foundation under grant DPP 92-21395 and under previous grants for research at Siple station, Antarctica.

The Editor thanks T. Ondoh and one other referee for their assistance in evaluating this paper.

References

Bullough, K., and J. L. Sagredo, VLF goniometer observations at Halley Bay, Antarctica, I, The equipment and the measurement of signal bearing, *Planet. Space Sci.*, *21*, 899, 1973.

Carpenter, D. L., Fast fluctuations in the arrival bearing of magnetospherically propagating signals from the Siple, Antarctica, VLF transmitter, *J. Geophys. Res.*, *85*, 4157, 1980.

Carpenter, D. L., Remote sensing of the magnetospheric plasma by means of whistler mode signals, *Rev. Geophys.*, *26*, 535, 1988.

Hayakawa, M., T. Okada, and A. Iwai, Direction findings of medium-latitude whistlers and their propagation characteristics, *J. Geophys. Res.*, *86*, 6939, 1981a.

Hayakawa, M., Y. Tanaka, T. Okada, and A. Iwai, Goniometric direction finding for low-latitude whistlers and their propagation mechanism, *J. Geophys. Res.*, *86*, 6781, 1981b.

Hayakawa, M., Y. Tanaka, A. Iwai, J. Ohtsu, L. R. O. Storey, C. Beghin, and T. S. Jörgensen, Simultaneous spaced direction-finding measurements of medium-latitude VLF/ELF emissions, *Planet. Space Sci.*, *29*, 505, 1981c.

Hayakawa, M., Y. Tanaka, S. S. Sazhin, T. Okada, and K. Kurita, Characteristics of dawnside mid-latitude VLF emissions associated with substorms as deduced from the two-stationed direction finding measurements, *Planet. Space Sci.*, *34*, 225, 1986.

Hayakawa, M., K. Ohta, and S. Shimakura, Spaced direction finding of nighttime whistlers at low and equatorial latitudes and their propagation mechanism, *J. Geophys. Res.*, *95*, 15,091, 1990.

Ikeda, M., K. Tsuruda, and S. Machida, Exit areas of VLF waves inferred from the multistation measurements at Roberval, Canada, *J. Geomagn. Geoelectr.*, *40*, 227, 1988.

Ladwig, J. M., and A. R. W. Hughes, An asymmetry in the direction of arrival of whistlers at Sanae, Antarctica, *J. Atmos. Terr. Phys.*, *51*, 61, 1989.

Leavitt, M. K., D. L. Carpenter, N. T. Seely, R. R. Padden, and J. H. Doolittle, Initial results from a tracking receiver direction finder for whistler mode signals, *J. Geophys. Res.*, *83*, 1601, 1978.

Machida, S., and K. Tsuruda, Intensity and polarization characteristics of whistlers deduced from multi-station observations, *J. Geophys. Res.*, *89*, 1675, 1984.

Madden, M. A., M. J. Rycroft, and N. E. Smith, Ground-based ELF/VLF observations at high latitudes during passes of GEOS-1 and ISEE-1 and -2, *Space Sci. Rev.*, *22*, 465, 1978.

Matthews, J. P., A. J. Smith, and I. D. Smith, A remote unmanned ELF/VLF goniometer receiver in Antarctica, *Planet. Space Sci.*, *27*, 1391, 1979.

Mechtly, E. A., Accuracy of rocket measurements of lower ionosphere electron concentrations, *Radio Sci.*, *9*, 373, 1974.

Nagano, I., M. Mambo, and I. Kimura, Estimation of collision frequency in the upper *D* and *E* regions from LF wave by means of a rocket experiment, *J. Geomagn. Geoelectr.*, *34*, 27, 1982.

Nagano, I., M. Mambo, T. Shimbo, and I. Kimura, Intensity and polarization characteristics along the Earth's surface for the ELF-VLF waves emitted from a transmission cone in the high latitude, *Mem. Natl. Inst. Polar Res. Spec. Issue Jpn.*, *42*, 34, 1986.

Nagano, I., M. Mambo, T. Shimbo, and I. Kimura, Propagation characteristics in the Earth-ionosphere waveguide for VLF waves emitted from trapping cones at high latitudes, *Mem. Natl. Inst. Polar Res. Spec. Issue Jpn.*, *47*, 183, 1987.

Nishino, M., Y. Tanaka, A. Iwai, and T. Hirasawa, A new direction finding technique for auroral VLF hiss based on the measurement of time differences of arrival at three spaced observing points, *Planet. Space Sci.*, *29*, 365, 1981.

Ohta, K., M. Hayakawa, and Y. Tanaka, Ducted propagation of daytime whistlers at low latitudes as deduced from ground-based direction findings, *J. Geophys. Res.*, *89*, 7557, 1984.

Ohta, K., M. Hayakawa, and S. Shimakura, Frequency dependence of arrival direction and polarization of low-latitude whistlers and their ducted propagation, *J. Geophys. Res.*, *94*, 6975, 1989.

Okada, T., A. Iwai, and M. Hayakawa, The measurement of incident and azimuthal angles and the polarization of whistlers at low latitudes, *Planet. Space Sci.*, *25*, 233, 1977.

Okada, T., A. Iwai, and M. Hayakawa, A new whistler direction finder, *J. Atmos. Terr. Phys.*, *43*, 679, 1981.

Ondoh, T., M. Kotaki, T. Murakami, S. Watanabe, and Y. Nakamura, Propagation characteristics of low-latitude whistlers, *J. Geophys. Res.*, *84*, 2097, 1979.

Sagredo, J. L., and K. Bullough, VLF goniometer observations at Halley Bay, Antarctica, II, Magnetospheric structure deduced from whistler observations, *Planet. Space Sci.*, *21*, 913, 1973.

Smith, A. J., and D. L. Carpenter, Echoing mixed-path whistlers

near the dawn plasmapause, observed by direction-finding receivers at two Antarctic stations, *J. Atmos. Terr. Phys.*, *44*, 973, 1982.

Strangeways, H. J., M. J. Rycroft, and M. J. Jarvis, Multi-station VLF direction-finding measurements in eastern Canada, *J. Atmos. Terr. Phys.*, *44*, 509, 1982.

Tanaka, Y., and M. Nishino, The propagation of auroral hiss observed on the ground as deduced from direction-finding measurements, *Planet. Space Sci.*, *36*, 259, 1988.

Tsuruda, K., and K. Hayashi, Direction finding technique for elliptically polarized VLF electromagnetic waves and its application to the low-latitude whistlers, *J. Atmos. Terr. Phys.*, *37*, 1193, 1975.

Tsuruda, K., and M. Ikeda, Comparison of three different types of VLF direction-finding techniques, *J. Geophys. Res.*, *84*, 5325, 1979.

Tsuruda, K., S. Machida, T. Terasawa, A. Nishida, and K. Maezawa, High spatial attenuation of the Siple transmitter signal and natural VLF chorus observed at ground-based chain stations near Roberval, Quebec, *J. Geophys. Res.*, *87*, 742, 1982.

Xu, J. S., M. Tian, C. C. Tang, M. Hayakawa, K. Ohta, and S. Shimakura, Direction finding of night-time whistlers at very low latitudes in China: Preliminary results, *Planet. Space Sci.*, *37*, 1047, 1989.

D. L. Carpenter, VLF/STAR Laboratory, Durand, Room 323, Stanford University, Stanford, CA 94305. (e-mail: tsstar::carpenter)

M. Ikeda, Section of General Education, Musashi University, Nerima-Ku, Tokyo 176, Japan.

I. Nagano and T. Shimbo, Department of Electrical and Computer Engineering, Kanazawa University, Kanazawa 920, Japan.

(Received September 13, 1993; revised October 17, 1994; accepted October 17, 1994.)